Astron. Astrophys. 343, 111–119 (1999)

ASTRONOMY AND ASTROPHYSICS

Time-dependent photoelectric absorption, photoionization and fluorescence line emission in gamma-ray burst environments

Markus Böttcher[1], **Charles D. Dermer**[2], **Anthony W. Crider**[1], **and Edison P. Liang**[1]

[1] Department of Space Physics and Astronomy, Rice University, 6100 S. Main St., Houston, TX 77005-1892, USA
[2] E.O. Hulburt Center for Space Research, Code 7653, Naval Research Laboratory, Washington, DC 20375-5352, USA

Received 18 September 1998 / Accepted 2 December 1998

Abstract. If γ-ray bursts are associated with dense star-forming regions in young galaxies, photoelectric absorption by the dense circumburster material (CBM) will occur. As the burst evolves, the surrounding material is photoionized, leading to fluorescence line emission and reduced photoelectric absorption opacity. We have analyzed this process in detail, accounting for the time-dependent photoelectric absorption, photoionization and fluorescence line emission from the CBM. We find that even if GRBs are hosted in dense star-forming regions, photoionization of the GRB environment leads to a constant, but very weak level of delayed fluorescence line emission on timescales of weeks to years after the burst. A temporally evolving iron K edge absorption feature can serve as diagnostic tool to reveal the density structure of the CBM and may provide an opportunity for redshift measurements. We also investigated whether photoelectric absorption could be responsible for the spectral evolution of the low-energy slopes of some bright BATSE γ-ray bursts displaying extremely hard spectra below the peak energy, inconsistent with the optically-thin synchrotron shock model. We find that a very strong metal enrichment (~ 100 times solar-system abundances) in the γ-ray burst environment and a rather peculiar spatial distribution of the CBM would be necessary in order to account for the observed hard spectra below a few 100 keV and their temporal evolution.

Key words: atomic processes – radiative transfer – gamma rays: bursts – X-rays: bursts

1. Introduction

The recent discovery of X-ray and optical afterglows of γ-ray bursts as a result of the Italian-Dutch BepoSAX mission (e.g., Costa et al. 1997; Metzger et al. 1997; van Paradijs et al. 1997; Kulkarni et al. 1998) has given strong support for the cosmological blastwave model for γ-ray bursts (Rees & Mészáros 1992; Mészáros & Rees 1993; Katz 1994). The observed temporal decay of the afterglow emission, generally well described by a power-law $F_\nu(t) \propto t^{-\alpha}$ with $1.1 \lesssim \alpha \lesssim 1.5$ (Costa et al. 1997; Feroci et al. 1998; Piro et al. 1998a) and the overall spectral shape of the afterglow emission are in very good agreement with optically thin synchrotron emission by relativistic electrons accelerated at a relativistic blast wave as it expands and sweeps up matter from the surrounding medium (e. g., Katz 1994, Tavani 1996, Wijers, Rees & Mészáros 1997, Dermer & Chiang 1998).

If γ-ray bursts are associated with the collapse of massive objects (e. g., Paczyński 1998), they are expected to be correlated with dense star-forming regions and are possibly located within them. Recent comparisons of the GRB flux distribution with the star-formation history of the early universe seem to support this hypothesis (Wijers et al. 1998). If this is true, photoelectric absorption, photoionization and fluorescence line emission in the vicinity of γ-ray bursts will inevitably occur and might lead to observable consequences. Recently, Mészáros & Rees (1998) have qualitatively discussed absorption edges and line features from atoms irradiated by a blastwave evolving in the nonradiative regime, for both a low denstiy interstellar medium or a dense burst environment which might be appropriate for the hypernova scenario (Paczyński 1998). They suggest that for reasonable parameter values absorption edges as well as fluorescence lines and resonance-scattered burst emission could be detectable with future, rapid follow-up observations of GRB afterglows. They also propose that the non-detection of optical afterglows for some bursts for which X-ray afterglows have been observed and precisely located by the BeppoSAX satellite, could be due to photoelectric absorption and extinction by gas and dust in the GRB environment. Ghisellini et al. (1998) have discussed the detectability of the iron K edge and Kα fluorescence line in this context and suggested that it might provide a possibility to measure the redshift of GRBs. They also predict that the Fe Kα line should still be detectable long after the continuum X-ray afterglow has faded away.

The process of time-dependent photoionization and photoelectric absorption has been studied in detail by Perna & Loeb (1998). They focus on optical absorption lines originating in the CBM and point out the effect that photoionization of the GRB environment by the burst radiation leads to a reduction of the absorption opacity, and suggest the temporal evolution of absorption line shapes and equivalent widths as a new diagnostic tool to map the GRB environment. This method is applicable in the case of very dense GRB environments, in which case the evolution of the absorption line shapes occurs on a sufficiently

Send offprint requests to: M. Böttcher

short timescale to be measurable within the short periods during which optical GRB afterglows remain observable.

In this paper, we focus on the observable effects in the X-ray regime of the time-dependent photoelectric absorption, photoionization and fluorescence line emission processes in the vicinity of a cosmological γ-ray burst. We adopt a similar approach to the one used by Perna & Loeb (1998), but additionally implementing the Auger process and fluorescence line emission following inner-shell ionization events. We calculate the temporal evolution of the absorbed burst spectrum, present light curves of the continuum and fluorescence line emission, and suggest observational tests to reveal the density structure of GRB environments on the basis of GRB follow-up X-ray observations.

Another motivation for this work is the finding (Crider et al. 1997; Preece et al. 1998) that the temporally resolved low-energy spectra of many γ-ray bursts during the early phases of the burst are inconsistent with optically thin synchrotron emission from ultrarelativistic electrons. This latter process gives an energy spectral index ($F_\nu \propto \nu^\alpha$) $\alpha = 1/3$ if electrons in the blast wave are inefficiently cooled, maintaining an ultrarelativistic low-energy cutoff (Katz 1994) and $\alpha = -1/2$ if synchrotron cooling is efficient, yielding an electron power-law spectrum in energy with index $p = -2$. A significant fraction of snapshot burst spectra have differential slopes harder than 1/3 at the low-energy end of sensitivity range of the BATSE instrument (Preece et al. 1998), and in these bursts the low-energy spectra generally evolve from hard to soft during the decay phase of the burst radiation (Crider et al. 1997). We investigated whether photoelectric absorption of the intrinsic γ-ray burst spectrum in the vicinity of the GRB could be responsible for the hard low-energy spectra of GRBs and their temporal evolution. This process has first been studied in the context of the low-energy spectra of γ-ray bursts by Liang & Kargatis (1994). Considering the photoelectric absorption of an unbroken power-law spectrum by pure neutral iron along the line of sight to a GRB, they found that an absorption depth at the iron K edge of several hundred is necessary to account for the steep γ-ray burst spectra if the intrinsic spectrum is an unbroken power-law with the spectral index observed above the break. Assuming a solar-system abundance of iron in the absorbing matter, this corresponds to a Thomson depth of $\tau_T \gtrsim 100$, which would result in strong distortion of the high-energy spectrum due to Compton downscattering. They therefore concluded that this scenario may be ruled out. Using our detailed photoionization calculations, we have re-investigated this idea under more realistic assumptions, and basically confirm the previous results of Liang & Kargatis (1994).

In Sect. 2, we describe the model assumptions and the computational procedure which we use to solve the time-dependent photoionization and radiative transfer problem. We discuss the expected evolution of photoelectric absorption features and the luminosity and light curves of fluorescence lines under various assumptions for the density in the GRB environment in Sect. 3. In Sect. 4 we present a short discussion on the application of our code to the low-energy spectra of time-resolved BATSE GRB spectra. We summarize and present our conclusions in Sect. 5.

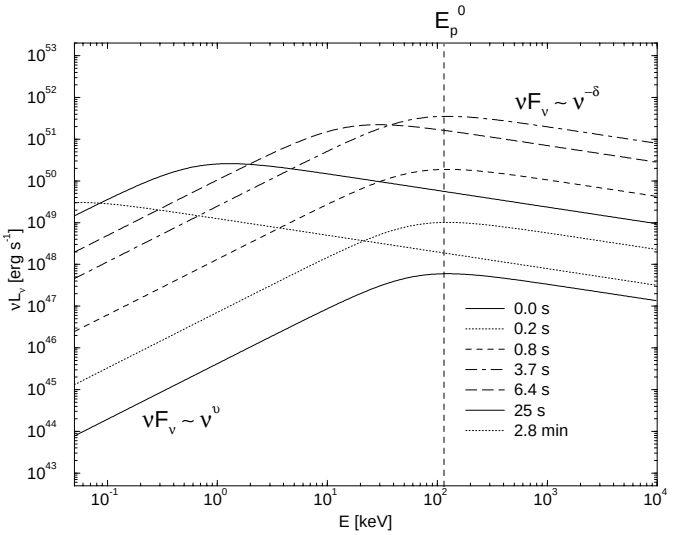

Fig. 1. Evolution of the intrinsic (unabsorbed) model GRB spectrum. Parameters: $E_0 = 10^{54}$ erg, $\Gamma_0 = 300$, $g = 1.6$, $\eta = 0$, $\upsilon = 4/3$, $\delta = 0.4$.

2. Model assumptions and computational scheme

We simulate a relativistic blast wave expanding into and irradiating and photoionizing a stationary external medium. The evolution of the blast wave and of the spectrum radiated by it is represented by the analytic parametrization of Dermer et al. (1998). The spectral evolution of our intrinsic model GRB spectra is illustrated in Fig. 1.

The model is determined by the following parameters: $E_0 = 10^{54}\, E_{54}$ erg is the total energy transferred to relativistic baryons during the initial explosion, and Γ_0 is the initial bulk Lorentz factor of the ejecta forming the relativistic blast wave. The term υ is the spectral index of the νF_ν spectrum below the spectral break (we use $\upsilon = 4/3$, corresponding to optically thin synchrotron emission from a relativistic electron population), and δ is the spectral index above the break (we use $\delta = 0.4$ in our calculations; our final results are insensitive to this value). The radius of the blast wave at a given time is denoted by r_b. As the blast wave moves into the external medium, it sweeps up external matter and starts to decelerate when the energy of swept-up external matter in the rest frame of the blast wave equals the rest-mass energy of the initial ejecta. The radius at which this happens is denoted r_d, the deceleration radius. Beyond this point, the bulk Lorentz factor Γ of the blast wave decreases according to a power-law in radius, determined by the deceleration index g, i. e. Γ evolves as

$$\Gamma(r_b) = \begin{cases} \Gamma_0 & \text{for } r_b < r_d \\ \Gamma_0 \left(\frac{r_b}{r_d}\right)^{-g} & \text{for } r_d \le r_b \le r_d\, \Gamma_0^{1/g} \end{cases} . \qquad (1)$$

The CBM is assumed to have a power-law profile in distance from the burst, determined by the density n_0 at the deceleration radius and the power-law index η:

$$n_{ext}(r) = n_0 \left(\frac{r}{r_d}\right)^{-\eta} . \qquad (2)$$

The abundances of atoms and ions of the various elements are characterized by the abundance coefficients $X_a^i(r,t)$, where the subscript a characterizes the element, and the superscript i characterizes the ionization state. The density of a given element a in ionization state i is given by $n_a^i(r,t) = n_{ext}(r)\, X_a^i(r,t)$. Initially, we assume all elements in the external medium to be neutral and no metallicity gradients, though the element abundances are allowed to differ from standard solar-system abundances. In our calculations, we include H, He, C, N, O, Ne, Mg, Si, S, Ar, Ca, Fe, and Ni, and neglect other elements.

We start our simulation at $r_b \ll r_d$, i. e. at a point in time where the flux of the gamma-ray burst radiation is yet far below its maximum value. We split the external medium up into a radial grid with steps Δr. Within each radial zone we calculate the absorption optical depth due to photoionization,

$$\Delta\tau_{abs}(r,E) = \Delta r\, n_{ext}(r) \sum_{a,i} X_a^i(r)\, \sigma_a^i(E), \tag{3}$$

where the photoionization cross sections $\sigma_a^i(E)$ of all atoms and ions are evaluated using the relevant subroutines of the XSTAR code (Kallman & Krolik 1998; Kallman & McCray 1982). The atoms and ions in each radial zone will be photoionized by the incident radiation. As the solution is advanced by a time step Δt in the stationary frame, it will take a time interval $\Delta t_{rec} = \Delta t\,(1-B)$, where $B = \sqrt{1-1/\Gamma^2}$, until the radiation from the blast wave emitted at the next time step reaches a fixed point. Thus, we assume that the zone located at radius r is illuminated for a time step Δt_{rec} by the constant incident spectrum $F_E(r,E) = L_E(r,E)\, e^{-\tau_{abs}(r,E)}/(4\pi\, r^2)$. Each ionization state will be depopulated as

$$\left(\frac{dX_a^i(r,t)}{dt}\right)_- = -X_a^i(r,t) \int dE\, \frac{F_E(r,E)}{E} \sigma_a^i(E). \tag{4}$$

Radiative transitions following a photoionization event will result in a large variety of fluorescence lines. We include 200 strong fluorescence lines from N, O, Ne, Mg, Si, S, Ar, Ca, Fe, and Ni, using the ionization-state dependent fluorescence yields and line energies given in Kaastra & Mewe (1993). We assume that all fluorescence lines are emitted isotropically at the location of the photoionization event. This leads to temporally delayed fluorescence line emission as seen by the observer: The fluorescence line radiation from an atom or ion located at a distance r from the center, at an angle θ relative to the line of sight to the observer, will be observed $\Delta t_{fl} = (1-\cos\theta)\, r/c$ later than the spherical light front which has photoionized the atom or ion.

Due to the high probability of Auger transitions following a K- or L-shell ionization of heavy atoms or ions, each photoionization event may result in effectively ejecting several electrons from the atom or ion. For this reason, e. g., it takes on average typically only 12, rather than 26 hard X-ray photons to ionize a neutral Fe atom completely. This is accounted for by means of a transition probability matrix, describing the probability $P_a^{i,j}$ of transition from ionization state i to any higher ionization state j after photoionization of an ion (a,i). (Without the Auger process, $P_a^{i,j} = \delta_{i+1,j}$.) The evaluation of this probability matrix requires the knowledge of the probability of a K-, L(s)-, and L(p)-shell photoionization, which is calculated using the respective (sub)shell photoionization cross sections, and the probabilities for an Auger transition following the respective ionization events, as a function of the number of ejected Auger electrons. For the elements with nuclear charge $Z \le 18$, approximate values of these probabilities can be found in Weisheit (1974), while for the higher-Z elements the fluorescence and Auger yields are taken from Kaastra & Mewe (1993).

The higher ionization states ($j > 1$) will be populated due to ionization of lower-ionized ions according to

$$\left(\frac{dX_a^j(r,t)}{dt}\right)_+ = \sum_{i<j} P_a^{i,j}\, X_a^i \int dE\, \frac{F_E(r,E)}{E} \sigma_a^i(E). \tag{5}$$

Since the radiation field of the GRB is very intense and the density of surrounding material is assumed to be low ($n \lesssim 10^6\,\mathrm{cm}^{-3}$), recombination may be neglected in our simulations. We also neglect the effect of resonant scattering of fluorescence line emission because we are mostly interested in inner-shell fluorescence lines (in particular the Kα lines) which are generally non-resonant.

We solve iteratively the system consisting of Eqs. (4), (5), and the exponential depletion of the incident radiation field due to photoelectric absorption. This scheme is propagated through all radial zones until the outer boundery of our model system is reached and the radiation is assumed to escape freely towards the observer. After each time step, the solution is forwarded a time step Δt, in which the blast wave moves out a distance $\Delta r_b = c\, B\, \Delta t$. In the receiving (observer's) frame, this corresponds to a time step $\Delta t_{rec} = \Delta t\,(1-B)$. The new r_b is used to re-calculate the burst emission, and the emitted spectrum is processed through the volume still located outside r_b according to the scheme described above.

3. Absorption edges and delayed fluorescence line emission

A fraction Y, the fluorescence yield, of all K-shell ionization events of a certain element will be followed by a radiative transition, resulting in the emission of a fluorescence line photon. For the heavy elements Ca, Fe and Ni, the Kα transition is the most probable radiative transition following a K-shell ionization. As mentioned in the previous section, fluorescence line emission will be observable from virtually all parts of the GRB environment, while only a small solid angle $\sim 1/\Gamma^2$ of the blast wave contributes significantly to the observed radiation as long as the blast wave is highly relativistic. This leads to a time delay between the direct burst radiation and the fluorescence line emission from misaligned directions of the burst environment, which will contribute most of the fluorescence line fluence resulting from the burst if, as we are assuming throughout this paper, the GRB emission is uncollimated.

The maximum time delay of this fluorescence line emission may be estimated from the size of the ionization sphere of the GRB, which is the region where a certain element is essentially completely ionized. In a dense environment (which we call the optically thick limit), the ionization radius is determined by the

supply of photons with energies above the ionization threshold of the element under consideration. This radius is found by multiplying the number

$$N_a = X_a \int_0^{r_{ion}} d\tilde{r}\, 4\pi\, \tilde{r}^2 n_{ext}(\tilde{r}) \tag{6}$$

of atoms or ions in the ionization sphere by the number of photons $N_{a,ion}$ required to completely ionize an atom, and equating this result with the number of ionizing photons emitted during the burst. We obtain

$$r_{ion}(\text{opt. thick}) = \left(\frac{3\, k\, E_0\, \epsilon_K^{1-w}}{4\pi\, N_{a,ion}\, m_e\, X_a\, n_0\, (w-1)} \right)^{1/3}, \tag{7}$$

where k is a normalization factor,

$$k = \begin{cases} 0.33\, \epsilon_p^{w-2} & \text{in the non-radiative limit } (g = 3/2), \\ 0.30\, \epsilon_p^{w-2} & \text{in the radiative limit } (g = 3), \end{cases} \tag{8}$$

$\epsilon_p = E_p^0/(m_e c^2)$ is the normalized photon energy of the peak of the νF_ν spectrum at the peak of the burst light curve, $\epsilon_K = E_K/(m_e c^2)$ is the normalized K-edge energy, and $w = 3(2\,g+1)/(4\,g+\eta/2)$. Here, we have assumed that the K-edge energy is much smaller than the peak of the νF_ν spectrum of the burst in the early phase of the burst, i. e. $\epsilon_K \ll \epsilon_p$.

In a dilute environment (which we call the optically thin limit), the ionization radius is determined by the probability for an atom in the CBM to be ionized by a photon of the GRB radiation, which translates to the condition

$$\int_{\epsilon_K}^{\infty} d\epsilon\, \sigma_a(\epsilon)\, \frac{N_{ph}(\epsilon)}{4\pi r_{ion}^2} = 1. \tag{9}$$

This yields

$$r_{ion}(\text{opt. thin}) = \left(\frac{k\, E_0\, A_0\, \epsilon_K^{1-w}}{4\pi\, m_e\, Z^2\, [2+w]} \right)^{1/2}, \tag{10}$$

where Z is the nuclear charge of an atom/ion of species a and we have approximated the photoionization cross section by $\sigma_a(\epsilon) \approx (A_0/Z^2)\,(\epsilon/\epsilon_K)^{-3}$, where $A_0 = 6.3 \cdot 10^{-18}$ cm^2 and $\epsilon_K \approx 2.66 \cdot 10^{-5}\, Z^2$.

The delay timescale for fluorescence line emission is given by $\tau_{fl} = r_{ion}/c$. The expressions for the optically thin and optically thick limits are joined smoothly. In Fig. 2, the size of the ionization radius of hydrogen and iron is plotted as a function of the external density for standard parameters with the solar-system iron abundance of $X_{Fe} = 3.16 \cdot 10^{-5}$. The figure demonstrates that extremely long afterglow durations are expected from fluorescence line emission. The actual duration of the afterglow will generally be determined by the physical size over which the CBM has a substantial density, rather than by the supply of ionizing photons from the γ-ray burst. This corresponds to an expected fluorescence line afterglow duration of order months to years even if the GRB is associated with a dense star-forming region.

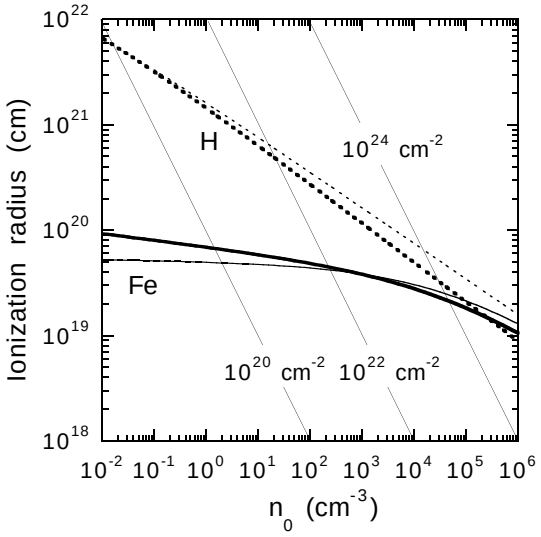

Fig. 2. The delay timescale of fluorescence line emission of iron and hydrogen ionized by a GRB evolving in the radiative limit (thick curves) and in the non-radiative limit (light curves), respectively, in a uniform external medium as a function of external density n_0. Parameters: $\Gamma_0 = 300$, $\upsilon = 4/3$, $\delta = 0.4$, $E_0 = 10^{54}$ erg, standard solar-system iron abundance.

The flux in fluorescence lines during this afterglow phase is expected to remain roughly constant over the entire duration of the fluorescence line afterglow because the volume from which fluorescence line emission can be observed at any given time scales as $\Delta V \propto r^2\, \Delta r \propto t^2\, \Delta t$, where Δt is the duration of the prompt GRB emission. This volume is illuminated by a continuum flux which scales as $F \propto r^{-2} \propto t^{-2}$ (only the outermost light fronts will be significantly affected by photoelectric absorption; thus, the illuminating fluence spectrum is basically the intrinsic burst spectrum), and a constant fraction A of this flux is absorbed and re-radiated in fluorescence lines. Thus, $L_{fl} \propto A\, F\, \Delta V \approx const.$

Figs. 3 and 4 demonstrate the results of numerical simulations for the case of a dilute, uniform medium with $n_0 = 10$ cm^{-3} extending out to a distance of $r_{max} = 10$ kpc from the location of the explosion. This might be representative of the case that the GRB is hosted within a galaxy, but not directly inside a star-forming region. Here we use the standard parameters for the intrinsic GRB spectrum as quoted in the previous section. Fig. 3 shows the observable GRB spectra for various observing times. An iron absorption edge around 7 keV is visible. Even in the late afterglow phase the burst spectrum remains heavily absorbed below a few keV. On the scale adopted in this figure, only a weak fluorescence Kα line complex of oxygen at 0.52 — 0.58 keV is visible. In Fig. 4, we plot the light curves of the energy flux in Fe Kα fluorescence line emission compared to the continuum fluxes in the same energy band and at hard X-rays (40–50 keV). In agreement with our analytical estimate, the fluorescence line flux stays on a basically constant level until the time delay to the GRB equals the light travel time through the ionized medium. However, as is also obvious from Figs. 3 and 4, the expected flux of this long-duration line afterglow is

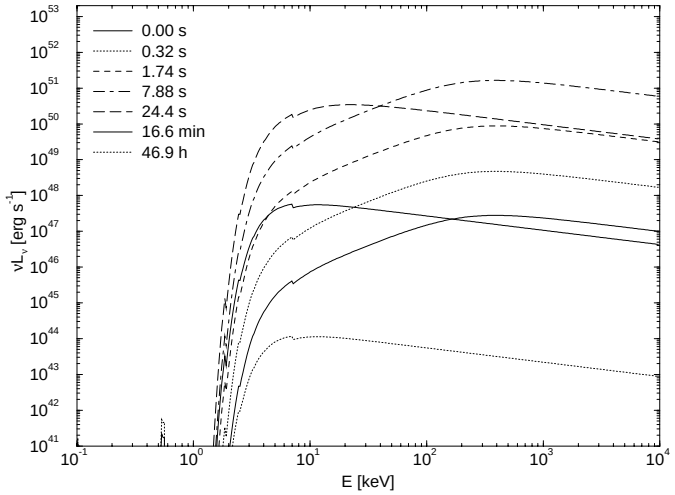

Fig. 3. Temporal evolution of the observed GRB spectra at various times after the initial explosion. Parameters: $n_0 = 10$ cm^{-3}, $r_{max} = 10$ kpc, $\Gamma_0 = 300$, standard solar-system element abundances.

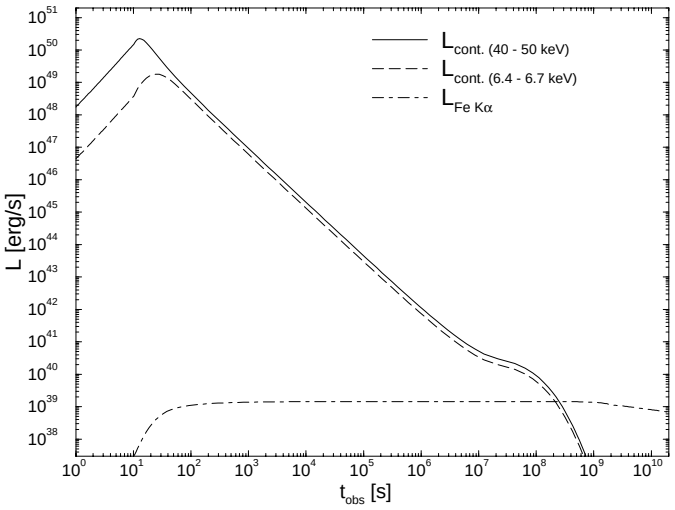

Fig. 4. Energy flux light curves in the iron Kα line band and in the hard X-ray continuum for the GRB spectral evolution shown in Fig. 2.

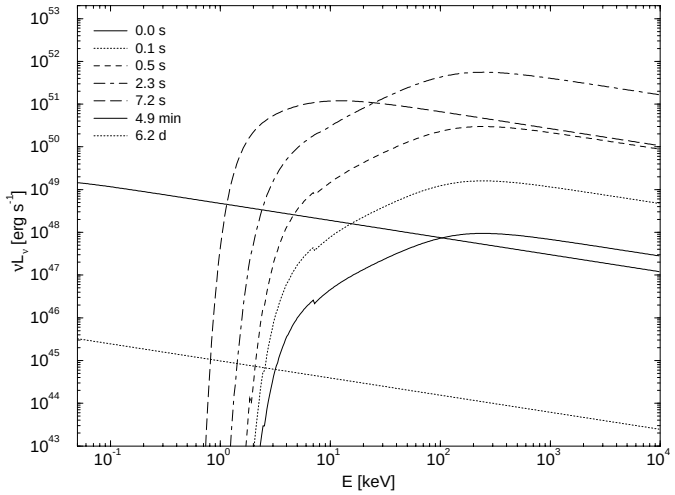

Fig. 5. Temporal evolution of the observed GRB spectra at various times after the initial explosion. Parameters: $n_0 = 10^5$ cm^{-3}, $r_{max} = 1$ pc, $\Gamma_0 = 150$, standard solar-system element abundances.

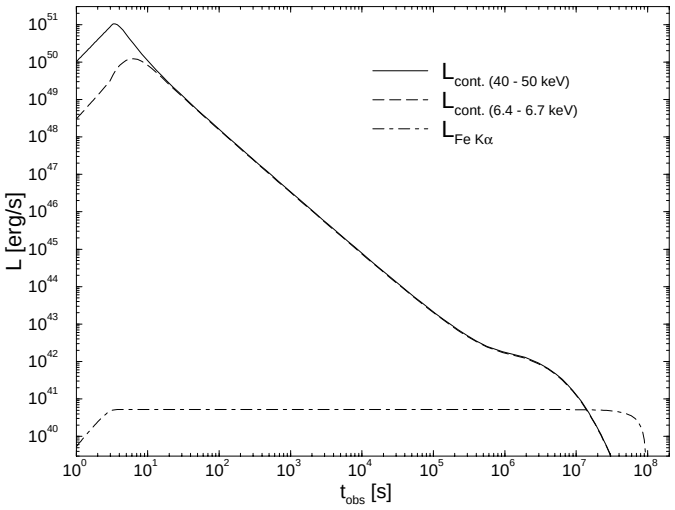

Fig. 6. Energy flux light curves in the iron Kα line band and in the hard X-ray continuum for the GRB spectral evolution shown in Fig. 4.

very low compared to the prompt burst emission. For a GRB located at $z = 1$, the luminosity shown in Fig. 4 translates into a flux of $F_{Fe\,K\alpha} \sim 6 \cdot 10^{-19}$ erg cm^{-2} s^{-1} (where we adopted $H_0 = 75$ km s^{-1} Mpc^{-1}, $q_0 = 0.5$, $\Lambda = 0$).

Figs. 5 and 6 illustrate the spectral evolution of a GRB in a dense environment, more appropriate to a star-forming region. Here, we assume a uniform external matter density of $n_0 = 10^5$ cm^{-3}, extended out to $r_{max} = 1$ pc. $\Gamma_0 = 150$ is used; all the other parameters are the same as for the previous example. Fig. 5 reveals that in this case the environment is photoionized rapidly because most of the absorbing material is very close to the GRB and therefore receives a very large ionizing flux, implying that it becomes optically thin to photoelectric absorption very quickly. This results in the rapid disappearance of the iron K absorption edge after ~ 1 s. After ~ 1.8 min., the CBM becomes optically thin to photoelectric absorption at virtually all frequencies. The fluorescence line flux stays on a constant level over a timescale of one light travel time through the ionized region (~ 3 years in our example). At a redshift of $z = 1$, the iron Kα fluorescence line flux is $F_{Fe\,K\alpha} \sim 3 \cdot 10^{-17}$ erg cm s^{-1} over ~ 5 yr. Note that the times quoted in all figures refer to the reference frame at the redshift of the burst.

As in the case of optical absorption lines investigated by Perna & Loeb (1998), we find that due to photoionization in a dense GRB environment any X-ray absorption features (with the Fe K edge being the most prominent one) will disappear rapidly after the onset of the GRB, on timescales which are anti-correlated with the external matter density and positively correlated with the size of the region over whith the CBM is extended. The detection of a varying Fe K edge in GRB X-ray spectra therefore provides a means not only to measure the redshift of the GRB independently (only if the edge significantly varies, however, can one be sure that the absorption happens in

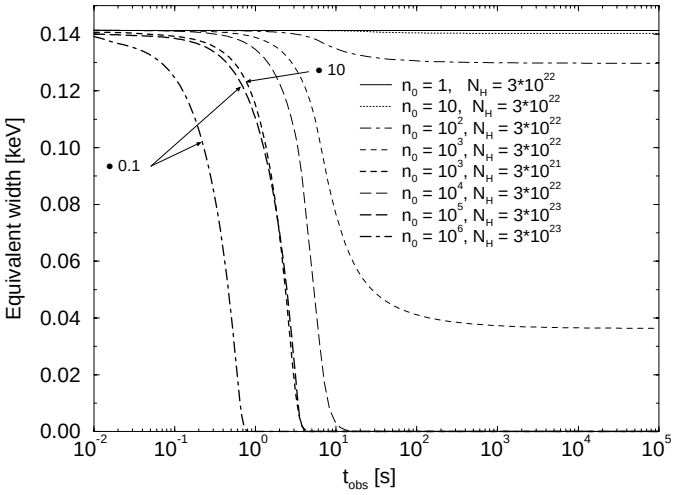

Fig. 7. Temporal evolution of the equivalent width of the iron K edge for different values of the CBM density (n_0 in units of cm^{-3}) and the hydrogen column density (N_H in units of cm^{-2}). Standard GRB parameters and solar-system iron abundance ($X_{Fe} = 3.16 \cdot 10^{-5}$) are used. The curve with $N_H = 3 \cdot 10^{21}$ cm^{-2} is multiplied by a factor of 10, the curves with $N_H = 3 \cdot 10^{23}$ cm^{-2} are multiplied by a factor 0.1 for clarity.

the CBM), but also to map the density structure of the GRB environment. In Fig. 7 we have plotted the temporal evolution of the equivalent width

$$EW = \int_{E_K}^{\infty} dE \, \left(1 - e^{-\tau_{abs}[E]}\right) \tag{11}$$

of the iron K edge for various combinations of the density and hydrogen column density (assuming standard solar-system abundances) of the CBM. The figure demonstrates that the necessity to observe a time-varying Fe K edge restricts this technique for measuring redshifts to fairly dense environments ($n \gtrsim 100$ cm^{-3}, $r_{max} \lesssim 100$ pc) in which the evolution of the Fe K edge is expected to be observable. Note that in any case the evolution of the Fe K edge happens on a timescale of $\lesssim 10$ s. It therefore appears to be subject to the same principal restrictions as the detection of optical absorption lines and requires rapid follow-up X-ray observations of γ-ray bursts and moderate spectral resolution at energies $\gtrsim 1$ keV during the prompt phase of the GRB.

In contrast, the fluorescence Fe-line emission is observed on very long time scales. In order to follow fluorescence line afterglows of GRBs, no fast slewing of an X-ray telescope is required or even helpful since they stay at a constant flux over timescales of months to years. The fluorescence line flux only dominates over the continuum flux from the burst after several months in the calculation shown. However, we find that even for very dense GRB environments the fluorescence line fluxes will hardly be detectable even with upcoming X-ray satellite missions such as AXAF or XMM: a flux of 10^{-16} erg cm^{-2} s^{-1} in the Fe Kα line (which is a very optimistic estimate), corresponding to $\sim (1+z) \cdot 10^{-8}$ photons cm^{-2} s^{-1}, observed with an instrument having an effective area of a few 100 cm^2 at the red-shifted line energy with an exposure of 100 ksec would yield $\lesssim 1$ count. The fluorescence line fluxes are strongly limited by the fact that the hydrogen column density towards the GRB is restricted to $N_H \ll 10^{24}$ cm^{-2} since there is no evidence for Compton downscattering in the high-energy spectra and time profiles of GRBs.

The shape of the fluorescence line light curves we find in our simulations differs only slightly from the analytical results of Ghisellini et al. (1998), who find that the fluorescence line afterglow should decay as a power-law $F_{FeK\alpha}(t) \propto t^{-0.1}$ after a maximum shortly after the burst. We attribute this minor discrepancy to the fact that in the analytical treatment of Ghisellini et al. (1998) the effect of photoionization on the GRB environment is neglected. As mentioned earlier, the rapid photoionization of the CBM by the leading light fronts of the burst radiation renders the environment optically thin to photoelectric absorption to the later light fronts which therefore remain basically unabsorbed. Thus, the illuminating fluence spectrum received by any point in the CBM is basically the intrinsic, unabsorbed burst spectrum.

Perna & Loeb (1998) used a temporal decay of the afterglow emission of $F_\nu(t) \propto t^{-3/4}$, which yields a rather strong late-time dependence of the variation of the absorption features because most of the fluence from the burst is emitted in the afterglow. Our choice of parameters leads to a temporal decay with index $\gtrsim 1.1$, in agreement with observations, and a much less pronounced variation of the absorption and fluorescence line features at late times (Mészáros & Rees 1998). In particular, most of the variation in the Lyα absorption edge will occur on the time scale on which the peak of the νF_ν spectrum is above the Lyα edge energy, which is typically a few hours. This is also the reason why the variation in the Fe K edge equivalent width as plotted in Fig. 7 occurs on very short time scales, typically within the first few seconds of the burst.

The fluxes calculated here scale basically linearly with the total burst energy E_0. The recent redshift determinations of GRB 971214 (Kulkarni et al. 1998) and GRB 980703 (Djorgovski et al. 1998b) seem to indicate that GRBs are at large cosmological distances, and their total energy release is in excess of 10^{53} erg. The choice of $E_0 = 10^{54}$ erg, which we adopted in the two examples illustrated above, might therefore be representative of bright bursts.

4. The low-energy slopes of GRB spectra

In order to investigate whether the low-energy spectra of GRBs are consistent with an optically thin synchrotron spectrum depleted by photoelectric absorption, we have fitted time-resolved BATSE spectra of GRBs with a Band model (which is very similar to our analytical parametrization of the GRB spectrum), suffering photoelectric absorption in a neutral medium where the opacity is calculated using the model of Morrison and McCammon (1983). The asymptotic low-energy slope α is fixed to $-2/3$ (photon number index). For details of the fitting procedure, in the framework of an extensive study of the low-energy

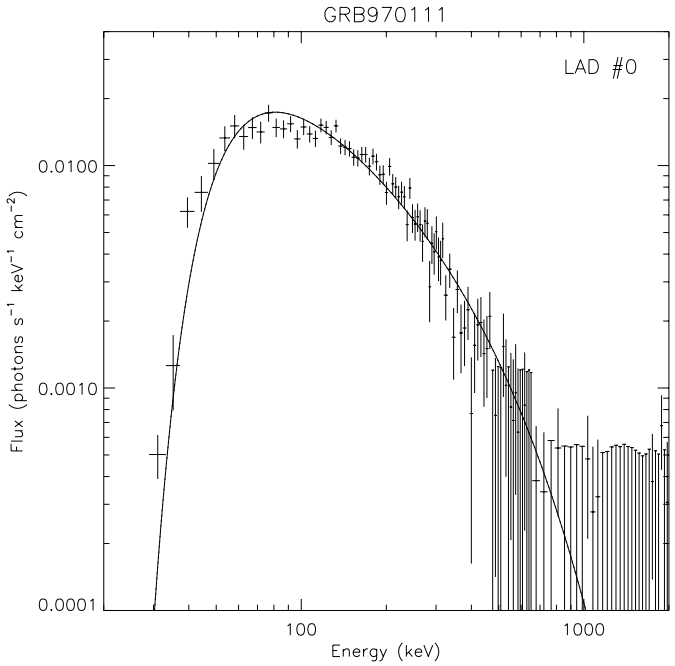

Fig. 8. Fit to a time-resolved BATSE spectrum of GRB 970111 using a Band model with photoelectric absorption. The spectrum is integrated from 0.029 to 2.112 s. The fit results in a neutral hydrogen column of $N_H = 1.83 \cdot 10^{26}\,\mathrm{cm}^{-2}$ (assuming solar-system abundances), corresponding to an absorption depth at the iron K edge of $\tau_K = 258$, and has a $\chi^2_\nu = 1.46$.

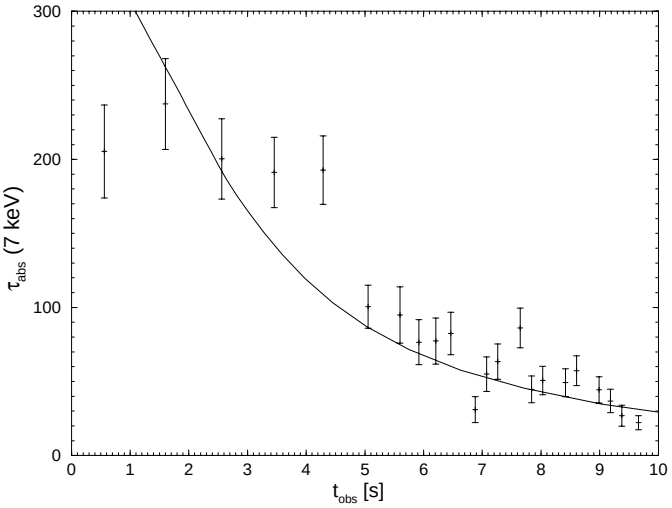

Fig. 9. Photoelectric absorption opacity at the Fe K-edge as a function of time. Parameters: $n_0 = 5 \cdot 10^6$ cm^{-3}, $r_{max} = 0.18$ pc, $\Gamma_0 = 100$, metal abundances = 100 × solar-system metal abundances. Data points are the values obtained from fits to the time-resolved BATSE spectra of GRB 970111.

spectra of BATSE GRBs, see Crider et al. (1998). One example of our fits to GRB 970111 using the Band model with photoelectric absorption is shown in Fig. 8. The fit has a reduced χ^2 of 1.46, and there appear to be systematic deviations at photon energies below ~ 100 keV. Furthermore, there were 10 time bins for which no fit with the photoelectric-absorption model was possible at all.

Our fits using an underlying $F_\nu \propto \nu^{1/3}$ spectrum at low X-ray frequencies indicate that slightly lower values of τ_0 are required in order to achieve acceptable fits to the data than in the situation investigated by Liang & Kargatis (1994), where the intrinsic burst spectrum was assumed to be a straight power-law. However, the fits still require $\tau_0 \gtrsim 100$ for the first few seconds of the burst. An example of the resulting τ_0 values is plotted in Fig. 9. Assuming a solar-system abundance of iron in the burst environment, this would correspond to a Thomson depth of $\tau_T \gtrsim 100$. Therefore the CBM would be highly opaque to Thomson downscattering and would cause any short-term fluctuations in the intrinsic burst radiation to be smeared out over a typical timescale $\Delta t \sim \tau_T\, r_{max}/c$. Both of these consequences of such a high τ_T are in obvious contradiction to the observations.

The above result suggests that the only way in which photoelectric absorption could efficiently affect the low-energy slopes of GRB spectra up to ~ 100 keV would be a strong enhancement of the iron abundance in the CBM. This could happen as the consequence of a metal enriched stellar wind produced by the GRB progenitor (which could be a supermassive star, causing the GRB in a hypernova explosion, see Paczyński 1998) and/or by massive stars in the vicinity of the GRB, if it is located in a star-forming region. The requirement that the Thomson depth of the CBM be $\lesssim 1$ implies that the iron enrichment relative to solar-system abundances in the burst environment would have to be of the order of 100. In order for the iron in the circumburst material to be completely photoionized within a few seconds, the metal-enriched matter must be highly concentrated around the burst location, $r_{max} \sim 0.2$ pc. For a metal enrichment factor of 100, this implies an average density in the immediate GRB environment of $n_0 \sim 5 \cdot 10^6$ cm^{-3}. We did a model simulation adopting such parameters, which roughly reproduces the temporal evolution of the photoionization opacity as required by the fits to the time-resolved BATSE spectra of GRB 970111. This is illustrated in Fig. 9.

Fig. 10 shows that this scenario would result in a considerable luminosity of delayed Fe Kα fluorescence line emission, dominating over the X-ray afterglow continuum after $\sim 2\,(1+z)$ days, which at $z = 1$ would translate into a line flux of $F_{FeK\alpha} \sim 10^{-14}$ erg cm^{-2} s^{-1}. This flux is still in agreement with the non-detection of Fe Kα line emission in any GRB X-ray afterglow observed so far, even those observed by ASCA (e.g., GRB 970228: Murakami et al. 1997, GRB 970828: Yoshida et al. 1997). A Fe Kα line flux of $\sim 10^{-14}$ erg cm^{-2} s^{-1}, corresponding to $\sim 2 \cdot 10^{-6}$ photons cm^{-2} s^{-1} at a photon energy of ~ 3.2 keV, would even be hard to detect, e.g., with the ACIS-S detector on board the AXAF satellite within a reasonable exposure time ($\lesssim 100$ ksec).

Thus, from the analysis of photoelectric absorption, photoionization and fluorescence line emission alone, the idea of the hard low-energy slopes of time-resolved BATSE GRB spectra being the result of photoelectric absorption in the CBM cannot be formally ruled out. However, the required extremely high

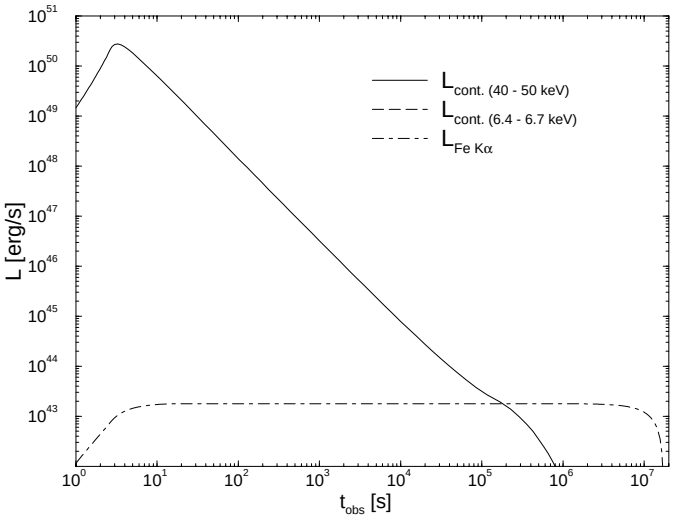

Fig. 10. Energy flux light curves in iron Kα lines and in two X-ray continuum bands resulting from the simulation reproducing the spectral evolution of GRB 970111 (Fig. 9). The continuum flux at 6.4–6.7 keV is too heavily absorbed to be visible on the scale of this plot.

metal enrichment and the peculiar spatial distribution necessary to reproduce the best-fit absorption depths look like fine-tuning and seem unlikely to be produced in a natural way. Furthermore, the fits to the time-resolved BATSE spectra of GRB 970111 with the photoelectric-absorption model were at best marginal. The BeppoSAX data on GRB 970111 (Feroci et al. 1998) constrain the photoelectric-absorption model severely, depending on the (unknown) redshift of this burst. In the fits presented above, the absorber was assumed to be located at $z = 0$. If the redshift of GRB 970111 is $z \gtrsim 1$, implying that the iron K edge is near or below the low-energy end of the BeppoSAX WFC energy range, then the 2 — 10 keV flux would have been heavily absorbed and thus undetectable by the WFC. Crider et al. (1998) show that in this case the combination of time-resolved BATSE spectra with simultaneous BeppoSAX data indicates that the photoelectric-absorption model is most likely inconsistent with the broadband X-ray spectrum of GRB 970111.

5. Summary and conclusions

We have analyzed the effects of photoionization, photoelectric absorption and fluorescence line emission in the vicinity of cosmological γ-ray bursts. Under the assumptions that the GRB emission is isotropic and GRBs are hosted in galaxies, we have calculated the expected time-dependence of photoelectric absorption features in the X-ray afterglows of γ-ray bursts and the flux and light curves of fluorescence lines from the photoionized CBM.

We find that an Fe K edge is the most easily detectable signature of the CBM in the X-ray continuum afterglows of GRBs. If the effect of photoionization on the CBM is identified by virtue of a reduction of the optical depth at the iron K edge as the burst evolves, this absorption can be attributed to material in the immediate vicinity of the GRB and may serve as an independent redshift indicator, as well as a method to map the GRB environment. This method is applicable to a dense environments such as star-forming regions. In more dilute, extended environments, the flux of the GRB emission becomes too weak at large distances from the burst location to be efficient in terms of photoionization.

We find that the ionization sphere, out to which photoionization and subsequent fluorescence line emission are efficient, is typically determined by the size of the region of considerable density around the GRB. This implies that the fluorescence line flux will remain relatively constant over timescales of months to years. This implies that rapid follow-up observations of γ-ray bursts are not needed to search for fluorescence lines. Instead, if there is any chance at all to detect fluorescence line afterglows, the candidate host galaxies of GRBs should be monitored with a sensitive X-ray pointing instrument such as AXAF over weeks to years after the GRB.

The depth of the Fe K absorption edge yields a measure of the Fe column density of the CBM, while the rate of decrease of the absorption edge (if observable) yields an estimate of the average distance of the CBM from the burster, thus allowing an estimate of the density structure of the GRB environment. The level of fluorescence line flux relative to the peak flux of the GRB continuum is also related to the average density of the CBM. While most of the parameters determining the evolution of a GRB blastwave in the framework of the cosmological blastwave model may be deduced from the flux and fluence spectra and spectral evolution of the prompt GRB emission and the continuum afterglow (if the redshift of the source is known), the density of the CBM always remained a free parameter. The absorption edges and the fluorescence line afterglow predicted in this paper provide a method to map the density of material in the GRB environment. Observation of vanishing absorption edges and/or fluorescence lines following a GRB also provides a very accurate measure of the redshift of the GRB. If the redshift of the host galaxy could be measured independently, this could confirm or rule out the yet unproven claim that those GRBs which are spatially coincident with host galaxies (e.g., GRB 970508: Bloom et al. 1998, GRB 971214: Kulkarni et al. 1998, GRB 980613: Djorgovski et al. 1998a, GRB 980703: Djorgovski et al. 1998b) are actually located within the proposed host galaxy.

Our prediction of the flux level of the fluorescence line afterglows is based on the assumptions that (1) the respective GRB is located within the proposed host galaxy, (2) the GRB emission is isotropic, and (3) the CBM is isotropic. If the assumption (2) is not true, only a small solid angle of the CBM is photoionized by the GRB radiation, which is why only a comparatively small volume can contribute to the fluorescence line afterglow. Furthermore, since this volume is exclusively located at small angles to our line of sight, only small time delays result. Therefore, the fluorescence line emission will be overwhelmed by the bright continuum afterglow. An anisotropy of the CBM, in contrast, could greatly enhance the observable fluorescence line flux. The recent marginal detection of a red-shifted Fe Kα line in the X-ray afterglows of GRB 970508 (Piro et al. 1998b) and

GRB 970828 (Yoshida et al. 1998) might be an indication for strong anisotropy of the CBM.

We have re-analyzed the possibility of photoelectric absorption causing the hard low-energy slopes of time-resolved BATSE GRB spectra. The fits using this spectral form are at best marginal, and the density structure around the GRB needs to be fine-tuned in a rather unnatural way in order to reproduce the observed spectral evolution of the low-energy spectrum of GRB 970111. We therefore confirm earlier findings that alternative mechanisms are more likely to be responsible for the hard low-energy snapshot spectra of GRBs and their spectral evolution.

Acknowledgements. We wish to thank Jon C. Weisheit and Tim Kallman for helpful discussions. This work was partially supported by NASA grant NAG 5-4055.

References

Bloom J.S., et al., 1998a, GCN Circ. No. 30
Costa E., et al., 1997, Nat 387, 783
Crider A., Liang E.P., Smith I.A., et al., 1997, ApJ 479, L39
Crider A., et al., 1998, in preparation
Dermer C.D., Chiang J., Böttcher M., 1998, ApJ 513, in press (astro-ph/9804174)
Dermer C.D., Chiang J., 1998, New Astronomy 3, 157
Djorgovski S.G., et al., 1998a, GCN Circ. No. 114
Djorgovski S.G., Kulkarni S.R., Bloom J.S., et al., 1998b, ApJ, submitted (astro-ph/9808188)
Feroci M., Antonelli L.A., Guianazzi M., et al., 1998, A&A 332, L29
Ghisellini G., Haardt F., Campana S., et al., 1998, ApJ, submitted (astro-ph/9808156)
Kaastra J.S., Mewe R., 1993, A&AS 97, 443
Kallman T.R., Krolik J.H., 1998, The XSTAR User's Guide
Kallman T.R., McCray R.A., 1982, ApJS 50, 263
Katz J.I., 1994, ApJ 432, L107
Kulkarni S., et al., 1998, Nat 395, 35
Liang E.P., Kargatis V.E., 1994, ApJ 432, L111
Liang E.P., Kusunose M., Smith I.A., Crider A., 1997, ApJ 479, L35
Mészáros P., Rees M.J., 1993, ApJ 405, 278
Mészáros P., Rees M.J., 1998, MNRAS 299, L10
Metzger M.R., et al., 1997, Nat 387, 878
Morrison R., McCammon D., 1983, ApJ 270, 119
Murakami T., Ueda Y., Shibata R., et al., 1997, In: Meegan C.A., Preece R.D., Koshut T.M. (eds.) 4th Huntsville Symposium
Paczyński B., 1998, ApJ 494, L45
Perna P., Loeb A., 1998, ApJ 501, 467
Piro L., et al., 1998a, A&A 331, L41
Piro L., et al., 1998b, presentation at Gamma-Ray Bursts in the Afterglow Era, 3–6 November, 1998, Rome, Italy
Preece R.D., Briggs M.S., Mallozzi R.S., et al., 1998, ApJ, in press (astro-ph/9808184)
Rees M.J., Mészáros P., 1992, MNRAS 258, 41P
Tavani M., 1996, Phys. Rev. Letters 76, 3478
van Paradijs J., et al., 1997, Nat 386, 686
Weisheit J.C., 1974, ApJ 190, 735
Wijers R.A., Bloom J.S., Bagla J.S., Natarayan P., 1998, MNRAS 294, L13
Wijers R.A., Galama T.J., 1998, ApJL, in press (astro-ph/9805341)
Wijers R.A., Mészáros P., Rees M.J., 1997, MNRAS 288, L51
Yoshida A., Namiki M., Otani C., et al., 1997, In: Meegan C.A., Preece R.D., Koshut T.M. (eds.) 4th Huntsville Symposium
Yoshida A., et al., 1998, presentation at Gamma-Ray Bursts in the Afterglow Era, 3–6 November, 1998, Rome, Italy